

Improved Microwave Absorption Performance with Sustainable Porous Carbon/Carbon Nanotube Composites

Leonardo Iusuti de Medeiros^{a,b,*} , Nila Cecília de Faria Lopes Medeiros^{a,b} ,

Guilherme Frederico Bernardo Lenz e Silva^c, Rodrigo Gabas Amaro de Lima^a ,

Gisele Amaral-Labat^a , Alan Fernando Ney Boss^c, Maurício Ribeiro Baldan^a

^aInstituto Nacional de Pesquisas Espaciais (PG-E TE), São José dos Campos, SP, Brasil.

^bUniversidade Estadual de Santa Cruz (DCET), Ilhéus, BA, Brasil.

^cUniversidade de São Paulo, Escola Politécnica, São Paulo, SP, Brasil.

Received: March 28, 2022; Revised: July 10, 2022; Accepted: July 12, 2022

The great technological advancement in wireless communication systems and devices generated the problem of electromagnetic pollution. Developing lightweight, sustainable, and low-cost materials is necessary to minimize electromagnetic pollution. A sustainable porous carbon (PC) absorber material was obtained from the crude black liquor by a simple and low-cost synthesis, and combined with carbon nanotube (CNT), presenting excellent microwave attenuation results. The PC absorber at 20 wt.% filling ratio exhibited an intense reflection loss of -35.7 dB at 15.5 GHz, and bandwidth of 1.15 GHz for a thickness of 5.90 mm. By adding 0.2 wt.% of CNT, the reflection loss was -34.6 dB at 17.9 GHz, and a bandwidth of 1.54 GHz for 4.90 mm. The study reveals that the combination of PC and CNT improves the attenuation capacity, allows adjustment in the frequency range of the attenuation peak, and promotes thickness reduction. The results obtained allow us to advance studies in developing high-performance, sustainable, and low-cost microwave-absorbing materials.

Keywords: *Electromagnetic Interference, Porous Carbon, Carbon Nanotubes, Absorber, Permittivity.*

1. Introduction

Microwaves are very efficient for information transmission and are widely used in various communication technologies¹⁻⁵. However, microwaves also produce electromagnetic interference in equipment and devices and can affect human health⁶⁻¹⁰. Therefore, several research studies are focused on developing materials with the ability to mitigate or eliminate electromagnetic pollution¹¹⁻¹⁴. Many materials have already been applied in producing electromagnetic radiation absorbers, such as polymers, ceramics, metallics, and carbons, among others^{15,16}. Widely researched metallic particles, oxides, and ferrites, which reach high absorption values, are being used as additives in absorbent composites^{11,17}. However, they have limitations such as high density and low oxidation resistance, which are undesirable characteristics in many applications¹⁸.

Carbon materials, such as porous carbon (PC), graphene, and carbon nanotube (CNT) have excellent qualities such as tunable dielectric properties, low density, large surface area, chemical stability, and oxidation resistance¹⁹⁻²⁴. These properties qualify them as electromagnetic radiation absorber materials. However, despite their excellent microwave absorption results, large-scale sp² carbon allotropes such as graphene and CNT are no longer viable. Such carbons are expensive and difficult to produce on a large scale¹⁸.

Materials from sustainable sources like industrial waste might be applied in developing PC for different applications²⁵⁻²⁷. Features, such as low-cost and simple processing, are essential requisites in using waste. Furthermore, recent studies show the effects of PC on electromagnetic wave attenuation due to large surface area, by increasing interfacial polarization in the matrix where they are inserted²⁸⁻³². Thus, porosity also plays a relevant role in the electromagnetic properties of the final composite.

Black liquor is a by-product from the pulp and paper industry generated in large quantities in the Kraft pulping process^{33,34}. This by-product is considered highly polluting due to its high pH (12.5). In 2019, our research team successfully prepared absorbing materials from Kraft black liquor by using porosity control with a spheric polymeric template, the PMMA to adjust the permittivity of the material². Here, the production of sustainable PC was based on a simple preparation without the use of templates, and by avoiding the washing steps and the consequent generation of new wastes. Thus, the proposed methodology involves the integral use of Kraft black liquor. Moreover, the use of PC and CNT in the production of absorbing materials has been developed in the literature^{35,36}. Therefore, a composite with sustainable PC and CNT was prepared at different mass ratios.

In this work, the absorber material containing 20 wt.% PC presented a reflection loss of -35.7 dB at 15.5 GHz with

*e-mail: limedeiros@uesc.br

5.95 mm thickness, demonstrating strong material potential. In the quest to improve absorptive PC attenuation capacity, a small amount of 0.2 wt.% CNT was added to the material containing 20 wt.% (20PC+0.2CNT). Similar attenuation of -34.6 dB was observed even with the thickness reduced from 5.95 to 4.90 mm. The combined PC and small amounts of CNT enhance the tuning effect. It allows for the production of sustainable absorber materials of high-performance, lightweight, low-cost, and simple processing.

2. Experimental Section

2.1. Materials

The black liquor was kindly supplied by Suzano Papel e Celulose S.A, formaldehyde 37 wt.% P.A. NEON, resorcinol in Synth flakes, white silicone Redelease and multi-walled carbon nanotube by Cheap Tubes.

2.2. PC preparation and absorber composite

PC was prepared with 100 g of black liquor, 15 g of resorcinol, and 44 g of formaldehyde. Under constant stirring, at the temperature of 40 °C, the resorcinol was mixed with the black liquor until its complete dissolution, then formaldehyde is added until the solidification of the polymeric foam. The foam remains under atmospheric conditions for 3 days to complete the dry process. After this period, the material was carbonized in a tubular oven under an N₂ atmosphere up to 900 °C for 120 minutes. After carbonization, the material was crushed and classified in a sieve of 500 μm. The absorber composite was prepared by mechanically mixing in the proportions of 15 wt.% and 20 wt.% of PC in a silicone rubber matrix. The mixture was poured into molds produced in a 3D printer, with specific offset dimensions for Ku-band, varying from 2 to 6 mm. Concentrations of 15 and 20 wt.% are selected based on performed tests. Concentrations below 15 wt.% do not present significant microwave attenuations, while 20 wt.% is the saturation limit of PC into silicone rubber. Two sets of samples were analyzed, one containing PC in silicone matrix and a second batch adding 0.2 wt.% CNT to PC and silicone rubber.

Samples containing 15 wt.% and 20 wt.% of PC dispersed in silicone rubber, respectively, are named 15PC and 20PC. Samples containing 15 wt.% and 20 wt.% PC with the addition of 0.2 wt.% CNT dispersed in silicone rubber are named 15PC+0.2CNT and 20PC+0.2CNT, respectively.

2.3. Characterization of materials

Morphological and structural characterizations of carbon materials were performed by field-emission scanning electron microscopy (FEG-SEM), model Mira3-Tescan, X-ray diffraction (XRD) in a Rigaku, model Ultima IV CuK α radiation ($\lambda=0.15418$ nm) and Raman scattering spectroscopy, Horiba LabRam HR Evolution model at 514.5 nm. The specific surface area and pore volume values were obtained by a Micromeritics ASAP 2020 Plus and a mercury porosimetry (0.0035 – 414 MPa) Micromeritics AutoPore III, respectively. Electromagnetic properties, such as complex permittivity ($\epsilon=\epsilon'-j\epsilon''$) were obtained by vector network analyzer (VNA-N5235A from Keysight Technologies)

and rectangular Ku-band waveguide (model P11644A) in the frequency range from 12.4 to 18 GHz. The reflection loss was obtained using a metallic plate positioned at the back of the sample.

3. Results and Discussions

The morphology of the PC particles before the addition of CNT is seen in Figure 1a. The carbon particles present macropores (pores larger than 50 nm)³⁷ distributed on all surfaces. These pores are formed during the solidification and subsequent carbonization of black liquor foam. The process of obtaining the foam generates a large amount of heat, an exothermic reaction, where the increase in temperature promotes the volatilization of excess formaldehyde and water present in the black liquor, generating bubbles during the solidification of the foam. Structures with high porosity can contribute to increasing the microwave absorption performance of the material, generating polarization interfaces, and suppressing the eddy current effects³⁸. In addition, the presence of pores effectively reduces the density, making it possible to obtain a lighter material. Figure 1b shows the PC particles involved by CNTs. From a morphological point of view, the addition of CNT can create paths for electron displacement. The CNTs, when connected by the simple overlapping of the tubes, produce a vast network of ways through which the electrons can move freely. This effect can increase the conductivity of the composite causing conduction loss. Figure 1c shows the Raman spectra of PC and CNT particles. The band observed at approximately 1350 cm⁻¹ is called the D band, used to characterize the structural disorder caused by the defects existing in the crystalline structure of the carbon material. The band in the region of ~1580 cm⁻¹ is associated with the percentage of structural order, also called graphitization band or G-band^{39,40}. The intensity ratio of the bands (I_D/I_G) is a qualitative indicator of the defect density or degree of graphite of the materials^{40,41}. The fundamental difference in the intensity ratio between CNT and PC is associated with the size of a nanocrystallite and point defects in the sp² carbons. Considering the graphene, single-layer graphene (SLG) as a reference, the distance between defects, LD = 24 nm, is a measure of the amount of disorder. By changing the LD value, the ratio I_D/I_G changes. The LD calculated for CNT and PC are ~14 and 10 nm, respectively. These values indicate that the distance between defects in the CNT is greater than in PC, which affects the ratio of I_D/I_G . Besides the information on the peak intensity, a strong indication of the structural disorder can be obtained from the FWHM. By considering the defects that can activate the D peak, it is evident that CNT has lower FWHM than PC, which implies a lower number of defects. With a decrease in number of defects, the ratio I_D/I_G decreases. The broadening of the D peak may be associated with different types of defects⁴². Higher graphitization can improve the conductivity of the carbon material and increase the dielectric loss. However, it is not interesting to eliminate all defects, as they can act as polarization centers by increasing the polarization of electric dipoles⁴⁰. The XRD analysis of PC particles and CNT are revealed in Figure 1d. It can be observed that CNT exhibit their main peaks at ~25° and smaller peaks at ~44°, which are assigned to the crystalline planes (002) and (100),

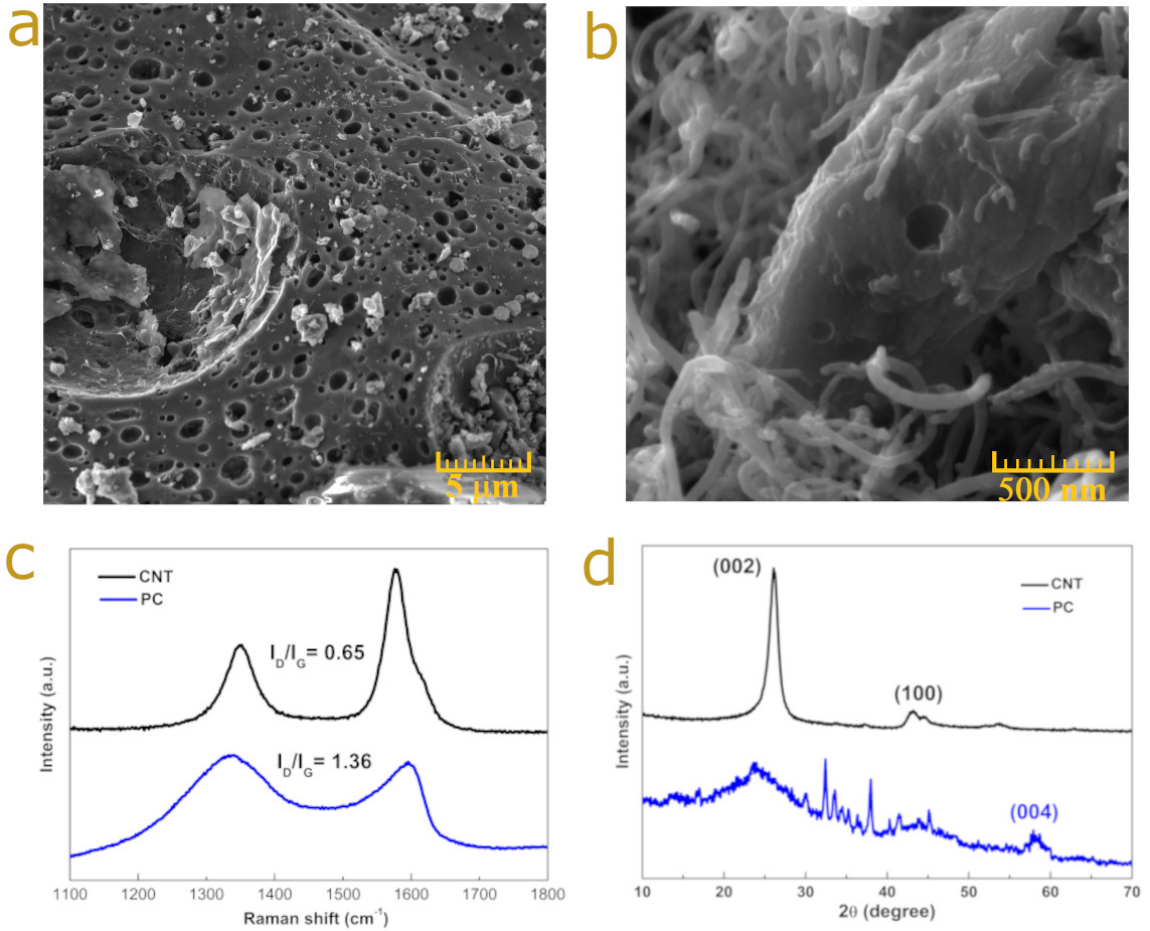


Figure 1. (a) PC particles; (b) PC particles with CNT; (c) Raman spectroscopy of the PC and CNT; (d) XRD of PC and CNT.

respectively^{2,27,35}. CNT still presents a small peak $\sim 57^\circ$ from a crystalline plane (004) related to the reflection of the second order of (001)^{36,43-45}. PC presents its bands centered at $\sim 24^\circ$ and $\sim 44^\circ$, a characteristic of amorphous carbon.

The specific surface area showed a typical value for the CNT, around $100 \text{ m}^2/\text{g}$ ⁴⁶⁻⁴⁸, while the PC showed no developed micro or mesoporosity (pores lesser than 50 nm) presenting a value of $11 \text{ m}^2/\text{g}$ (Table 1). The latter agrees with the porosity seen by SEM images, where macropores (pores larger than 50 nm) are observed. The synthesis parameters, such as polymerization reaction and the carbonization process assisted the formation of porous on a microscale range. These pores are characteristics of carbon foams⁴⁹⁻⁵¹ and are normally analyzed by mercury intrusion-extrusion curves.

Macroporosity analysis of PC particles was performed by mercury porosimetry analysis, and the results are shown in Table 2. The material presented a low bulk density (0.66 g/mL) and a high porosity (76%) indicating the lightweight property of the developed sustainable material. The porosity value is comparable to those from bio-sourced carbon aerogels that were obtained from multiple steps of preparation under supercritical conditions⁵²⁻⁵⁴. The mercury accumulated in the pores is related to the total volume of pores and the respective total macropore area ($82 \text{ m}^2/\text{g}$).

Table 1. Specific surface area (S_{BET}) and total volume of pores ($V_{0.99}$) of CNT and PC were calculated from N_2 adsorption-desorption isotherms.

Sample	S_{BET} ($\text{m}^2 \text{ g}^{-1}$)	$V_{0.99}$ ($\text{cm}^3 \text{ g}^{-1}$)
CNT	90	0.22
PC	11	-

Table 2. Textural properties of PC from mercury porosimetry: bulk density (ρ_b); skeletal density (ρ_s); porosity (ϕ); total volume of pores (V_{Hg}); total pore area (A_{total}) and pore diameter (ϕ).

Sample	ρ_b ($\text{g} \cdot \text{ml}^{-1}$)	ρ_s ($\text{g} \cdot \text{ml}^{-1}$)	ϕ (%)	V_{Hg} ($\text{ml} \cdot \text{g}^{-1}$)	A_{total} ($\text{m}^2 \cdot \text{g}^{-1}$)	ϕ (mm)
PC	0.66	2.70	76	1.14	82	99

Based on the porosimetry results, the process of synthesis to obtain PC is very efficient in the macropores production, showing pore diameters distributed on the microscale range and centered at $99 \mu\text{m}$.

Electromagnetic properties are tightly related to the relative complex permittivity ($\epsilon_r = \epsilon' - j\epsilon''$) and relative complex permeability ($\mu_r = \mu' - j\mu''$). The crucial impact on the electromagnetic wave absorption performance occurs,

especially in the relative complex permittivity (ϵ_c) that represents the loss caused by dielectric phenomena. The real part (ϵ') represents the storage capacity of electricity, while the imaginary part (ϵ'') represents the loss by dispersion of electricity^{55,56}. It is known that carbon materials do not have magnetic properties, and their attenuation capacity is governed only by the storage and dispersion of electricity⁵⁷.

The relative complex permittivity parameters in the frequency range 12.4 – 18 GHz of the samples are shown in Figure 2. The curves are similar for both real (ϵ') and imaginary (ϵ'') parts showing slight fluctuation. Samples 15PC are seen in Figure 2a, and present values of real permittivity (ϵ') close to 6.5 for all thicknesses and remain constant in the whole frequency range. Samples with the thickness of 3.80 and 4.85 mm present fluctuations in the region close to 17.0 and 14.6 GHz, respectively. These fluctuations might be associated with the interfacial polarization between PC and CNT, and intrinsic dipole polarization causing resonance peaks^{8,58}. Imaginary permittivity remains constant with a value close to 0.1 in the entire frequency range for all thicknesses, meaning that there is no energy consumption from the electromagnetic wave by the flow of electric current in the samples. The samples 15PC+0.2CNT are shown in Figure 2b. The increase of 0.2 wt.% of CNT did not promote relevant changes in the complex permittivity of the material when compared to 15PC without CNT. The (ϵ') and (ϵ'') values remained around 6.5 and 0.1 across

the frequency range. Resonance effects can be observed at 13.2 and 16.0 GHz on samples with 4.85 and 3.85 mm thicknesses. Figure 2c shows the complex permittivity of 20PC. An increase in (ϵ') values is observed at around 7.0. Resonance effects are observed in 3.95 and 5.00 mm at approximately 16.4 GHz and 13.2 GHz. The 5.95 mm sample showed an improvement in (ϵ'), reaching values greater than 7.8, suggesting an increase in the capability to store electric energy. In Figure 2d, the sample 20PC+0.2CNT did not show changes in the complex permittivity values, being around 7.0 (ϵ') and 0.1 (ϵ''). By comparing the samples 15PC+0.2CNT and 20PC+0.2CNT, we can conclude that the increase in (ϵ'), may be associated with increased PC concentration, as presented in the literature⁵⁹⁻⁶¹. Overall the frequency range and the (ϵ') constant behavior may be related to the orientation of electrical dipole polarization, which may be attributed to the increase in interface polarization that occurs with the increased PC concentration at the heterogeneous composite interface⁶²⁻⁶⁴. In other words, by increasing the PC from 15 wt.% to 20 wt.%, at the same CNT concentration, the interface between PC and CNT increases, resulting in enhanced interfacial polarization associated with storage capacity.

Based on the transmission line theory, reflection loss can be calculated to evaluate the microwave absorption performance of absorbers. For a single layer, the input impedance is given by

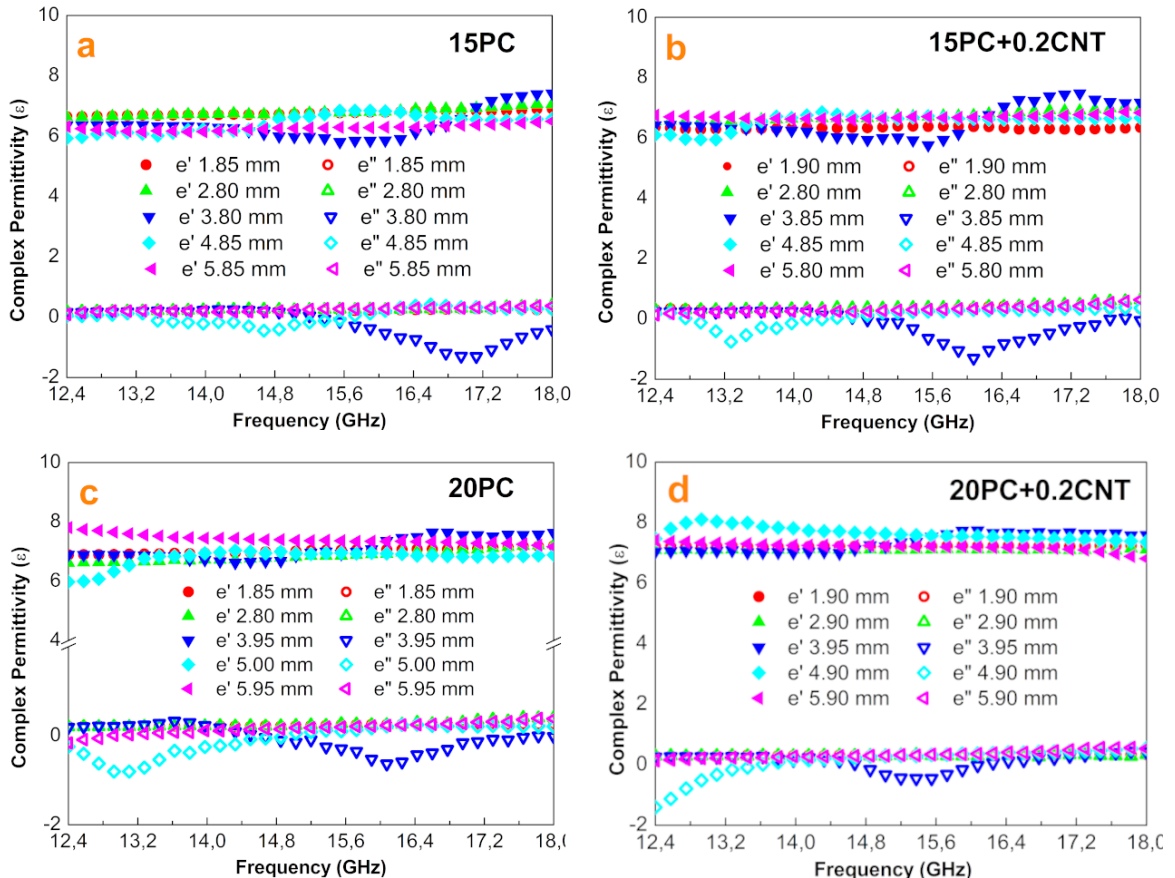


Figure 2. Complex permittivity: (a) 15PC; (b) 15PC+0.2CNT; (c) 20PC; (d) 20PC+0.2CNT.

$$Z_{in} = Z_0 \sqrt{\frac{\mu_r}{\epsilon_r}} \tanh(\gamma t)$$

Where $Z_0 = 377\Omega$ is the intrinsic impedance of free space, t is the thickness of the absorber, and γ is the propagation constant in the material

$$\gamma = \alpha + j\beta = j \frac{2\pi f}{c} \sqrt{\mu_r \epsilon_r}$$

where f is the frequency, c is the velocity of light, α denotes the attenuation, and β the phase constant.

The reflection loss is given by

$$RL = 20 \log \left| \frac{Z_{in} - Z_0}{Z_{in} + Z_0} \right|$$

The EM wave dissipation is associated with dielectric loss and magnetic loss. The magnetic losses are associated with domain wall, eddy current, and magnetic hysteresis losses. In our case, PC and CNT are not magnetic materials. Therefore, we can rule out a contribution from magnetic losses. Dielectric loss is related to interfacial polarization, defect-induced polarization, dipole/molecular polarization, electronic polarization, ionic polarization, and atomic polarization^{65,66}. Ionic, atomic, and electronic polarization are not present in the 2-18 GHz range. Homogeneous or heterogeneous interfaces can cause interfacial polarization or the Maxwell-Wagner-Sillars effect. Heterogeneous interfaces are associated with different materials. In our case, the PC

and CNT interface can be a source of interfacial polarization. Dipole polarization can occur in polar or nonpolar molecules under altering EM field, and defect-induced polarization can change the charge distribution leading to polarization.

The conductive loss is related to EM wave propagation in the material. By increasing ϵ'' , the alternate current (AC) conductive increases further enhancing conductive loss. The ionic and electronic polarization occurs in the ultraviolet or infrared region^{65,66}. The dielectric loss behavior can be explained by the Debye theory. A single Cole-Cole semicircle represents a Debye relaxation process. The number of the Cole-Cole semicircles can be associated with different polarization phenomena. A linear decrease was observed in the Cole-Cole semicircle, seen in Figure S1. In the frequency range (12.4-18 GHz), the rapidly changing field affects the polarization mechanism as frequency increases. Due to the field's switching direction, the net polarization can not keep up with the rapidly changing in the alternating field, decreasing its contribution. However, we can not rule out interfacial polarization due to heterojunctions between PC and CNT. Besides, a straight line may indicate a conduction loss.

Figure 3 shows the electromagnetic wave attenuation capacity of the materials. At low concentrations of PC, the sample 15PC reflection loss presents a non-significant attenuation of -8 dB at 16.7 GHz for the thickness of 5.85 mm, as observed in Figure 3a, as good absorber materials are associated with reflection loss lower than -10 dB. This value represents an attenuation of 90% of the incident electromagnetic radiation⁶⁷.

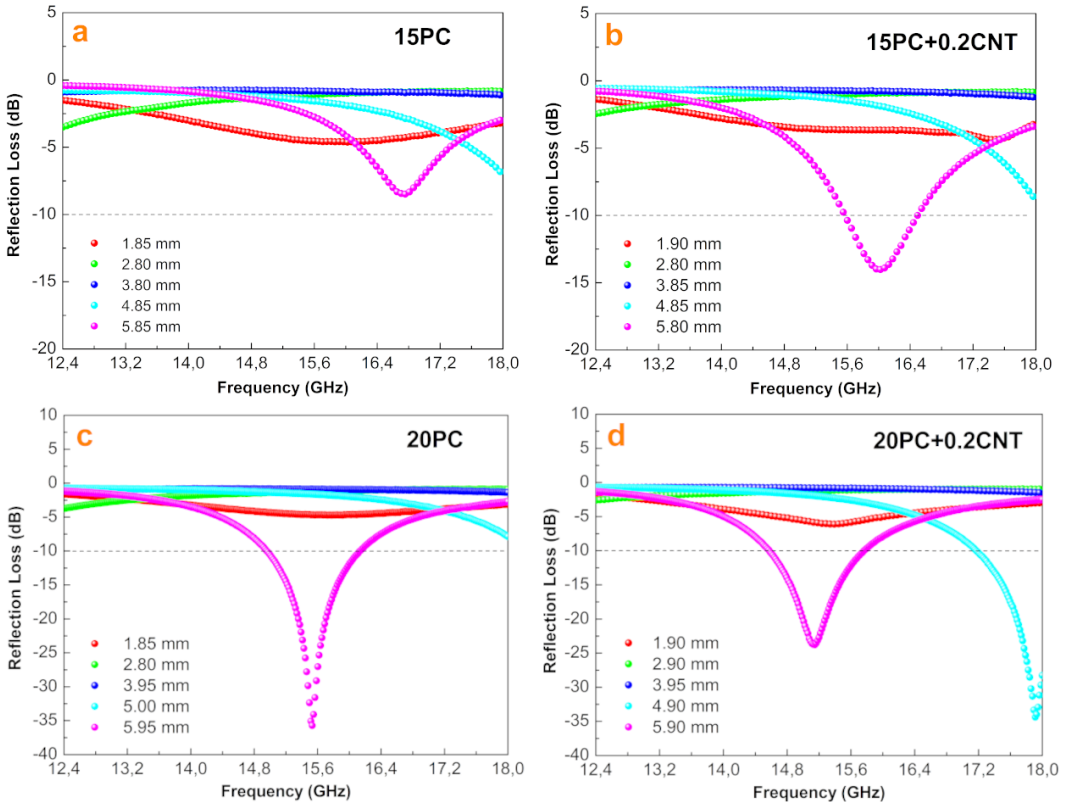


Figure 3. Reflection Loss: (a) 15PC; (b) 15PC+0.2CNT; (c) 20PC; (d) 20PC+0.2CNT.

The addition of a small proportion of CNT (0.2 wt.%) promoted an improvement in attenuation capacity reaching -14 dB at 16 GHz, as given in Figure 3b. The presence of CNT increased the attenuation of the material, probably due to the formation of new interfaces^{68,69}. When many interfaces arise between PC particles and CNT an increase in interfacial polarization is expected. This effect can arise when negative charges are distributed in CNTs, thus, in the presence of an electromagnetic field, space charges can be trapped causing the arising of a local electric field that will generate large interfacial polarization^{68,70,71}. Figure 3c shows the samples 20PC. At 5.95 mm a peak attenuation of -35.7 dB centered at 15.5 GHz is found. The increase in the concentration of PC particles shifted the reflectivity peak to lower frequencies, by a displacement of approximately 1.3 GHz compared to the 15PC sample. This effect may be related to increased real permittivity (ϵ')⁷² from 6.5 to 7.8. Materials with higher permittivity values are expected to have better absorption performance. The addition of 0.2 wt.% of CNT favored the presence of two peaks at 15.1 and 17.9 GHz, with attenuation of -23.92 and -34.6 dB, respectively, this result can be seen in Figure 3d. Finally, it is worth mentioning that the best electromagnetic wave attenuation can be achieved when the impedance matching condition is satisfied.

The excellent results obtained may be associated with the relationship between thickness and frequency, which can be explained by the cancellation model $\lambda/4$ according to

$$t_m = \frac{\lambda}{4\sqrt{|\epsilon_r||\mu_r|}} = \frac{nc}{4f_m\sqrt{|\epsilon_r||\mu_r|}} \quad (n=1,3,5,\dots)$$

where t_m is matching thickness, f_m is the frequency of the lowest reflection loss, λ the wavelength of the electromagnetic wave, c the velocity of light, ϵ_r the complex permittivity, and μ_r the complex permeability of the microwave absorber. When the thickness of the absorber material is equal to an odd multiple of one-quarter of the wavelength, the optimal reflection loss occurs^{73,74}. Once the incident electromagnetic wave enters the material and reaches the interface between the material and the perfect metal plate the wave will be reflected and canceled at the interface of the material.

The mitigation by cancellation model $\lambda/4$ might be responsible for the excellent performance obtained in samples 20PC+0.2CNT with thicknesses of 4.90 and 5.90 mm. Figure 4 correlates experimental reflection loss thickness and t_m thickness calculated based on the cancellation model $\lambda/4$. The calculated thickness values were aligned with the experimental reflectivity results obtained for thicknesses 4.90 and 5.90 mm. The overlap of the calculated experimental and theoretical results reinforces the possible contribution of the attenuation mechanism by the cancellation model $\lambda/4$ in

our results. Since the peaks come from the cancellation model, we can infer that absorbers with a thickness of $t < 4.90$ mm, have no frequencies within the $\lambda/4$ model, indicating that no reflection loss peak exists in the curve. Besides the attenuation mechanism, the EM wave dissipation may be associated with dielectric loss. The Debye relaxation process is analyzed to investigate the dielectric loss source. In the supplementary material, we include the Cole-Cole plot, Figure S1. A linear decrease was observed for the sample 20PC+0.2CNT. Two dominant mechanisms may be related to dielectric loss, interfacial polarization, which is associated with polarization relaxation due to PC/CNT heterogeneous interfaces, and conduction loss enhanced by the addition of CNT. In other words, the dominant dielectric loss mechanism stems from interfacial polarization and conduction loss.

The results are compared with studies in the literature and the reflection loss is in the same order of magnitude as the PC, as presented in Table 3. The PC obtained in this work presented a reflection loss value of -35.7 dB, and bandwidth of 1.15 GHz in the sample 20PC at 5.95 mm thickness. Sample 20PC+0.2CNT shows a reflection loss

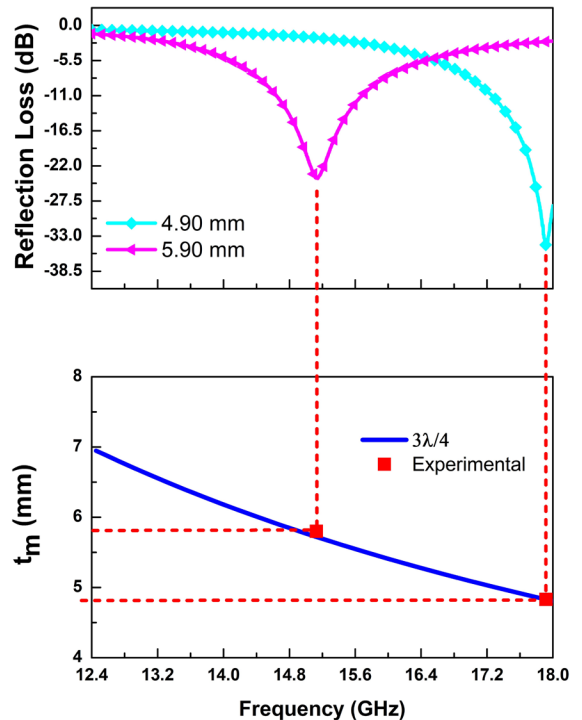


Figure 4. Sample 20PC+0.2CNT thickness of reflection loss corresponding to calculated t_m .

Table 3. Performance of some microwave absorbing materials.

Sample	Materials	Thickness (mm)	RL (dB)	Frequency (GHz)	Reference
20PC	Porous carbon	5.95	-35.7	15.5	This work
20PC+0.2CNT	Porous carbon/MWCNT	4.90	-34.6	17.9	This work
C3-15 wt.%	Porous carbon	2.00	-19.0	11.8	Flórez Vergara et al. ²
RHPC/Co	Porous carbon/Co	1.80	-40.1	10.7	Fang et al. ⁷⁵
RHPC/Fe	Porous carbon/Fe	1.40	-21.8	14.4	Fang et al. ⁷⁵
900CA	Porous carbon	1.9	-37.55	14.73	Wang et al. ⁷⁶

of -34.6 dB, attenuating 99.9% of the microwave and a bandwidth of 1.54 GHz at 4.90 mm thickness. The RHPC/Co samples have an attenuation of -40.1 dB and bandwidth of 2.7 GHz at 1.80 mm using PC and metal particles of Co, presenting a slightly higher value compared to this work. However, metal particles such as Co have a substantially high cost and a high density. Thus, the use of such metal increases both the cost and the weight of the composites. In addition, cobalt presents lower chemical stability than carbon materials.

The addition of only 0.2 wt.% CNT to PC reduced the thickness of the material by 1.05 mm and improved the bandwidth from 1.15 to 1.54 GHz compared to 20PC. The thickness reduction decreases the weight of the sample, meeting the requirement of light material.

4. Conclusion

In summary, this work showed the development of a PC material from the industrial by-product, the black liquor, in its integral form by using simple preparation steps without generating new wastes. The PC from Kraft black liquor proves to be quite viable, being obtained by simple synthesis and low-cost production, especially because this process also avoids industrial waste disposal.

The best results achieved an attenuation of -35 dB at 5.90 mm, and a bandwidth of 1.15 GHz for the sample 20PC. Increasing the PC concentration shifted the attenuation peak to lower frequencies and significantly improved microwave absorption. The addition of 0.2 wt.% CNT enhances the attenuation peak, shift effect increases bandwidth, and reduces material thickness resulting in the absorption of -34.6 dB at 4.90 mm, with a bandwidth of 1.54 GHz in sample 20PC+0.2CNT. Therefore, by adjusting the concentration of PC/CNT, it will be possible to control the intensity of absorption of electromagnetic radiation, shift the frequency range of attenuation, and scale the thickness of the material, showing the material's potential presented in this work.

5. Acknowledgments

The authors Leonardo Iusuti de Medeiros and Nila Cecília de Faria Lopes Medeiros thank Universidade Estadual de Santa Cruz – UESC and Instituto Nacional de Pesquisas Espaciais – INPE. This study was financed by the following Brazilian research agencies Coordenação de Aperfeiçoamento de Pessoal de Nível Superior - Brasil (CAPES) - Finance Code 001 and Financiadora de Estudos e Projetos – FINEP and CNPq.

6. Reference

- Wang J, Wu F, Yang Z, Shah T, Zhang A, Zhang Q, et al. Preparation of CTCNFs/Co₉S₈ hybrid nanofibers with enhanced microwave absorption performance. *Nanotechnology*. 2020;31(22):225605.
- Flórez Vergara DE, Kondo Lopes BH, Quirino SF, Silva GFBL, Boss AFN, Amaral-Labat GA, et al. Frequency selective surface properties of microwave new absorbing porous carbon materials embedded in epoxy resin. *Mater Res*. 2019;22:1-8.
- Ting TH, Wu KH. Synthesis, characterization of polyaniline/BaFe₁₂O₁₉ composites with microwave-absorbing properties. *J Magn Magn Mater*. 2010;322(15):2160-6.
- Cao M, Wang X, Cao W, Fang X, Wen B, Yuan J. Thermally driven transport and relaxation switching self-powered electromagnetic energy conversion. *Small*. 2018;14(29):1800987. <http://dx.doi.org/10.1002/smll.201800987>.
- Wu G, Cheng Y, Yang Z, Jia Z, Wu H, Yang L, et al. Design of carbon sphere/magnetic quantum dots with tunable phase compositions and boost dielectric loss behavior. *Chem Eng J*. 2018;333:519-28. <http://dx.doi.org/10.1016/j.cej.2017.09.174>.
- Huang L, Chen C, Li Z, et al. Challenges and future perspectives on microwave absorption based on two-dimensional materials and structures. *Nanotechnology*. 2020;31(16):162001.
- Liu X, Cui X, Chen Y, Zhang X-J, Yu R, Wang G-S, et al. Modulation of electromagnetic wave absorption by carbon shell thickness in carbon encapsulated magnetite nanospindles-poly(vinylidene fluoride) composites. *Carbon*. 2015;95:870-8.
- Wei B, Wang M, Yao Z, Chen Z, Chen P, Tao X, et al. Bimetallic nanoarrays embedded in three-dimensional carbon foam as lightweight and efficient microwave absorbers. *Carbon*. 2022;191:486-501.
- Zhao B, Deng J, Zhao C, Wang C, Chen YG, Hamidinejad M, et al. Achieving wideband microwave absorption properties in PVDF nanocomposite foams with an ultra-low MWCNT content by introducing a microcellular structure. *J Mater Chem C Mater Opt Electron Devices*. 2020;8(1):58-70.
- Folgueras LC, Nohara EL, Faez R, Rezende MC. Dielectric microwave absorbing material processed by impregnation of carbon fiber fabric with polyaniline. *Mater Res*. 2007;10(1):95-9.
- Huang L, Li J, Wang Z, Li Y, He X, Yuan Y. Microwave absorption enhancement of porous C@CoFe₂O₄ nanocomposites derived from eggshell membrane. *Carbon*. 2019;143:507-16.
- Huang Y, Wang Y, Li Z, Yang Z, Shen C, He C. Effect of pore morphology on the dielectric properties of porous carbons for microwave absorption applications. *J Phys Chem C*. 2014;118(45):26027-32.
- Kundi M, Ahlbom A, Green A, et al. Epidemiology of health effects of radiofrequency exposure. *Environ Health Perspect*. 2005;113(3):2004-5.
- Gupta S, Chang C, Lai C-H, Tai N-H. Hybrid composite mats composed of amorphous carbon, zinc oxide nanorods and nickel zinc ferrite for tunable electromagnetic interference shielding. *Compos, Part B Eng*. 2019;164:447-57.
- Wang G, Gao Z, Tang S, Chen C, Duan F, Zhao S, et al. Microwave absorption properties of carbon nanocoils coated with highly controlled magnetic materials by atomic layer deposition. *ACS Nano*. 2012;6(12):11009-17.
- Liu J, Che R, Chen H, Zhang F, Xia F, Wu Q, et al. Microwave absorption enhancement of multifunctional composite microspheres with spinel Fe₃O₄ cores and anatase TiO₂ shells. *Small*. 2012;8(8):1214-21.
- Cao MS, Yang J, Song WL, Zhang D-Q, Wen B, Jin H-B, et al. Ferroferric oxide/multiwalled carbon nanotube vs polyaniline/ferroferric oxide/multiwalled carbon nanotube multiheterostructures for highly effective microwave absorption. *ACS Appl Mater Interfaces*. 2012;4(12):6949-56.
- Kolanowska A, Janas D, Herman AP, Jędrzyński RG, Giżewski T, Boncel S. From blackness to invisibility: carbon nanotubes role in the attenuation of and shielding from radio waves for stealth technology. *Carbon*. 2018;126:31-52.
- Liu P, Zhang Y, Yan J, Huang Y, Xia L, Guang Z. Synthesis of lightweight N-doped graphene foams with open reticular structure for high-efficiency electromagnetic wave absorption. *Chem Eng J*. 2019;368:285-98.
- Ding Y, Zhang Z, Luo B, Liao Q, Liu S, Liu Y, et al. Investigation on the broadband electromagnetic wave absorption properties and mechanism of Co₃O₄-nanosheets/reduced-graphene-oxide composite. *Nano Res*. 2017;10(3):980-90.

21. Kim T, Lee J, Lee K, Park B, Jung BM, Lee SB. Magnetic and dispersible FeCoNi-graphene film produced without heat treatment for electromagnetic wave absorption. *Chem Eng J*. 2019;361:1182-9.
22. Hu Q, Yang R, Mo Z, Lu D, Yang L, He Z, et al. Nitrogen-doped and Fe-filled CNTs/NiCo₂O₄ porous sponge with tunable microwave absorption performance. *Carbon*. 2019;153:737-44.
23. Wu N, Lv H, Liu J, Liu Y, Wang S, Liu W. Improved electromagnetic wave absorption of Co nanoparticles decorated carbon nanotubes derived from synergistic magnetic and dielectric losses. *Phys Chem Chem Phys*. 2016;18(46):31542-50.
24. Chu W, Wang Y, Du Y, Qiang R, Tian C, Han X. FeCo alloy nanoparticles supported on ordered mesoporous carbon for enhanced microwave absorption. *J Mater Sci*. 2017;52(23):13636-49.
25. Zhao H, Cheng Y, Ma J, Zhang Y, Ji G, Du Y. A sustainable route from biomass cotton to construct lightweight and high-performance microwave absorber. *Chem Eng J*. 2018;339:432-41.
26. Zhao H, Cheng Y, Liu W, Yang L, Zhang B, Wang LP, et al. Biomass-derived porous carbon-based nanostructures for microwave absorption. *Nano-Micro Lett*. 2019;11(1):24.
27. Liang X, Liu R, Wu X. Biomass waste derived functionalized hierarchical porous carbon with high gravimetric and volumetric capacitances for supercapacitors. *Microporous Mesoporous Mater*. 2021;310:110659.
28. Hou L, Yang W, Jiang B, Wang P, Yan L, Zhang C, et al. Intrinsic defect-rich porous carbon nanosheets synthesized from potassium citrate toward advanced supercapacitors and microwave absorption. *Carbon*. 2021;183:176-86.
29. Zhang X, Cai L, Xiang Z, Lu W. Hollow CuS microflowers anchored porous carbon composites as lightweight and broadband microwave absorber with flame-retardant and thermal stealth functions. *Carbon*. 2021;184:514-25.
30. Cui J, Wang X, Huang L, Zhang C, Yuan Y, Li Y. Environmentally friendly bark-derived Co-Doped porous carbon composites for microwave absorption. *Carbon*. 2022;187:115-25.
31. Zhang X, Cheng J, Xiang Z, Cai L, Lu W. A hierarchical Co @ mesoporous C/ macroporous C sheet composite derived from bimetallic MOF and oxorylum indicum for enhanced microwave absorption. *Carbon*. 2022;187:477-87.
32. Wu YH, Peng K, Man Z, Zang R, Li P, Liu S, et al. A hierarchically three-dimensional CoNi/N-doped porous carbon nanosheets with high performance of electromagnetic wave absorption. *Carbon*. 2022;188:503-12.
33. Garron A, Arquilliere P, Maksoud W, Larabi C, Walter J-J, Santini CC. From industrial black liquor to pure phenolic compounds: a combination of catalytic conversion with ionic liquids extraction. *Appl Catal A Gen*. 2015;502:230. <http://dx.doi.org/10.1016/j.apcata.2015.06.012>.
34. Gouveia S, Fernández-Costas C, Sanromán MA, Moldes D. Polymerisation of Kraft lignin from black liquors by laccase from *Myceliophthora thermophila*: effect of operational conditions and black liquor origin. *Bioresour Technol*. 2013;131:288-94.
35. Yang X, Pang X, Cao M, Liu X, Li X. Efficient microwave absorption induced by hierarchical pores of reed-derived ultralight carbon materials. *Ind Crops Prod*. 2021;171:113814.
36. Kumar S, Ojha AK, Ahmed B, Kumar A, Das J, Materny A. Tunable (violet to green) emission by high-yield graphene quantum dots and exploiting its unique properties towards sun-light-driven photocatalysis and supercapacitor electrode materials. *Materials Today Communications*. 2017;11:76-86.
37. Bardestani R, Patience GS, Kaliaguine S. Experimental methods in chemical engineering: specific surface area and pore size distribution measurements—BET, BJH, and DFT. *Can J Chem Eng*. 2019;97(11):2781-91.
38. Wu YH, Peng K, Man Z, Zang R, Li P, Liu S, et al. A hierarchically three-dimensional CoNi/N-doped porous carbon nanosheets with high performance of electromagnetic wave absorption. *Carbon*. 2022;188:503-12.
39. DiLeo RA, Landi BJ, Raffaele RP. Purity assessment of multiwalled carbon nanotubes by Raman spectroscopy. *J Appl Phys*. 2007;101(6):064307.
40. Liu N, Dou Y, Zhang X, Yu L, Yan X. Design of porous FeNi-carbon nanosheets by a double-effect synergistic strategy for electromagnetic wave absorption. *Carbon*. 2022;190:125-35.
41. Oliveira AEF, Pereira AC, Bettio GB, Tarley CRT. Synthesis, studies and structural characterization of thermal and hydrazine reduction of graphene oxide by raman spectroscopy and infrared spectroscopy. *Rev Virtual Quím*. 2019;11(3):866-77.
42. Cançado LG, Jorio A, Ferreira EHM, Stavale F, Achete CA, Capaz RB, et al. Quantifying defects in graphene via Raman spectroscopy at different excitation energies. *Nano Lett*. 2011;11(8):3190-6.
43. Ungár T, Gubicza J, Ribárik G, Pantea C, Zerda TW. Microstructure of carbon blacks determined by X-ray diffraction profile analysis. *Carbon*. 2002;40(6):929-37.
44. Pawlyta M, Rouzaud JN, Duber S. Raman microspectroscopy characterization of carbon blacks: spectral analysis and structural information. *Carbon*. 2015;84:479-90.
45. Qiu T, Yang JG, Bai XJ, Wang Y-L. The preparation of synthetic graphite materials with hierarchical pores from lignite by one-step impregnation and their characterization as dye absorbents. *RSC Advances*. 2019;9(22):12737-46.
46. Harikrishna S, Robert AR, Ganja H, Maddila S, Jonnalagadda SB. A green, efficient and recoverable CeO₂/MWCNT nanocomposite catalyzed click synthesis of pyridine-3-carboxamides. *Appl Organomet Chem*. 2020;34(9):1-8.
47. Dai K, Shi L, Fang J, Zhang D, Yu B. NaCl adsorption in multi-walled carbon nanotubes. *Mater Lett*. 2005;59(16):1989-92.
48. Mahmoudi Alemi F, Mousavi Dehghani SA, Rashidi A, Hosseinpour N, Mohammadi S. Synthesize of MWCNT-Fe₂O₃ nanocomposite for controlling formation and growth of asphaltene particles in unstable crude oil. *Colloids Surf A Physicochem Eng Asp*. 2021;615:126295.
49. Wang F, Xu P, Shi N, Cui L, Wang Y, Liu D, et al. Polymer-bubbling for one-step synthesis of three-dimensional cobalt/carbon foams against electromagnetic pollution. *J Mater Sci Technol*. 2021;93:7-16.
50. Tondi G, Fierro V, Pizzi A, Celzard A. Tannin-based carbon foams. *Carbon*. 2009;47(6):1480-92.
51. Szczurek A, Fierro V, Plyushch A, Macutkevicius J, Kuzhir P, Celzard A. Structure and electromagnetic properties of cellular glassy carbon monoliths with controlled cell size. *Materials*. 2018;11(5):709. <http://dx.doi.org/10.3390/ma11050709>.
52. Szczurek A, Amaral-Labat G, Fierro V, Pizzi A, Masson E, Celzard A. The use of tannin to prepare carbon gels. Part I: carbon aerogels. *Carbon*. 2011;49(8):2773-84.
53. Szczurek A, Amaral-Labat G, Fierro V, Pizzi A, Celzard A. The use of tannin to prepare carbon gels. Part II. Carbon cryogels. *Carbon*. 2011;49(8):2785-94.
54. Braghiroli FL, Amaral-Labat G, Boss AFN, Lacoste, Pizzi. Tannin gels and their carbon derivatives: a review. *Biomolecules*. 2019;9(10):587.
55. Ji X, Zhang Y, Mo Y, Song Z, Wang Y, Yu J. Porous composites of vertical graphene sheets and Fe₃O₄ nanorods grown on Fe/Fe₃C particle embedded graphene-structured carbon walls for highly efficient microwave absorption. *J Alloys Compd*. 2022;905:164232.
56. Shen Y, Zhang F, Song P, Zhang Y, Zhang T, Wen X, et al. Design and synthesis of magnetic porous carbon nanofibers with excellent microwave absorption. *J Alloys Compd*. 2022;903:163971.
57. Fan D, Wei B, Wu R, Zhou J, Zhou C. Dielectric control of ultralight hollow porous carbon spheres and excellent microwave absorbing properties. *J Mater Sci*. 2021;56(11):6830-44.

58. Deng J, Wang Q, Zhou Y, Zhao B, Zhang R. Facile design of a ZnO nanorod-Ni core-shell composite with dual peaks to tune its microwave absorption properties. *RSC Advances*. 2017;7(15):9294-302.
59. Cao M-S, Cai Y-Z, He P, Shu J-C, Cao W-Q, Yuan J. 2D MXenes: electromagnetic property for microwave absorption and electromagnetic interference shielding. *Chem Eng J*. 2019;359:1265-302.
60. Ge C, Wang L, Liu G, Wang T, Chen H. Effects of particle size on electromagnetic properties of spherical carbonyl iron. *J Mater Sci Mater Electron*. 2019;30(9):8390-8.
61. Zhang S, Cao Q, Zhang M, Cai L, Yan Q. Effects of particle size on electromagnetic and microwave absorption properties of $\text{La}_{0.7}\text{Sr}_{0.3}\text{MnO}_{3.45}$ -epoxy composite. *Int J Appl Ceram Technol*. 2014;11(4):762-72.
62. Zhang X, Dong Y, Pan F, Xiang Z, Zhu X, Lu W. Electrostatic self-assembly construction of 2D MoS_2 wrapped hollow Fe_3O_4 nanoflowers@1D carbon tube hybrids for self-cleaning high-performance microwave absorbers. *Carbon*. 2021;177:332-43.
63. Liu Z, Pan F, Deng B, Xiang Z, Lu W. Self-assembled MoS_2 /3D worm-like expanded graphite hybrids for high-efficiency microwave absorption. *Carbon*. 2021;174:59-69.
64. Zhang Y, Zhang Y, Li Y, Yao M, Liu C, Miao X, et al. Facile design and permittivity control of reduced graphene oxide foam/ TiO_2 3D composite towards lightweight and high-efficient microwave absorption. *J Alloys Compd*. 2021;889:161695.
65. Chang Q, Liang H, Shi B, Wu H. Microstructure induced dielectric loss in lightweight Fe_3O_4 foam for electromagnetic wave absorption. *iScience*. 2022;25(3):103925.
66. Yadav K, Bagal R, Parmar S, Patro TU, Abhyankar AC. In situ coating of needle-like NiCo_2O_4 magnetic nanoparticles on lightweight reticulated vitreous carbon foam toward achieving improved electromagnetic wave absorption. *Ind Eng Chem Res*. 2021;60(39):14225-38.
67. Zhu Y, Guan X, Yang Z. One-pot synthesis of Carbon nanotube reinforced graphene aerogels and their applications in electromagnetic wave attenuation. *J Phys Chem Solids*. 2021;159:110279.
68. Li X, Wang L, Li X, Zhang J, Wang M, Che R. Multi-dimensional $\text{ZnO}@\text{MWCNTs}$ assembly derived from MOF-5 heterojunction as highly efficient microwave absorber. *Carbon*. 2021;172:15-25.
69. Guo S, Bao Y, Li Y, Guan H, Lei D, Zhao T, et al. Super broadband absorbing hierarchical CoFe alloy/porous carbon@carbon nanotubes nanocomposites derived from metal-organic frameworks. *J Mater Sci Technol*. 2022;118:218-28.
70. Li X, You W, Wang L, Liu J, Wu Z, Pei K, et al. Self-assembly-magnetized mxene avoid dual-agglomeration with enhanced interfaces for strong microwave absorption through a tunable electromagnetic property. *ACS Appl Mater Interfaces*. 2019;11(47):44536-44.
71. Cai C, Zhao Y, Xie S, Zhao X, Zhang Y, Xu Y, et al. Heterointerface-driven band alignment engineering and its impact on macro-performance in semiconductor multilayer nanostructures. *Small*. 2019;15(27):1900837. <http://dx.doi.org/10.1002/smll.201900837>.
72. Wang X, Gong R, Li P, Liu L, Cheng W. Effects of aspect ratio and particle size on the microwave properties of Fe-Cr-Si-Al alloy flakes. *Mater Sci Eng A*. 2007;466(1-2):178-82.
73. Chen N, Zhou J, Yao Z, Lei Y, Tan R, Zuo Y, et al. Fabrication of Nd-doped Ni-Zn ferrite/multi-walled carbon nanotubes composites with effective microwave absorption properties. *Ceram Int*. 2021;47(8):10545-54.
74. Guo S, Bao Y, Li Y, Guan H, Lei D, Zhao T. Structure-controlled Ni@N-doped porous carbon/carbon nanotube nanocomposites derived from metal-organic frameworks with excellent microwave absorption performance. *J Alloys Compd*. 2022;897:162737.
75. Fang J, Shang Y, Chen Z, Wei W, Hu Y, Yue X, et al. Rice husk-based hierarchically porous carbon and magnetic particles composites for highly efficient electromagnetic wave attenuation. *J Mater Chem C Mater Opt Electron Devices*. 2017;5(19):4695-705.
76. Wang K, Ye Z, Li X, Yang J. Nanoporous resorcinol-formaldehyde based carbon aerogel for lightweight and tunable microwave absorption. *Mater Chem Phys*. 2022;278:125718.

Supplementary material

The following online material is available for this article:

Figure S1 – Cole-Cole semicircle.